Neuron
Article

New Modules Are Added to Vibrissal Premotor Circuitry with the Emergence of Exploratory Whisking

Jun Takatoh,[1] Anders Nelson,[2] Xiang Zhou,[3] M. McLean Bolton,[4] Michael D. Ehlers,[5] Benjamin R. Arenkiel,[6] Richard Mooney,[2] and Fan Wang[1,*]
[1]Department of Cell Biology
[2]Department of Neurobiology
Duke University Medical Center, Durham, NC 27710, USA
[3]Department of Human Genetics, University of Chicago, Chicago, IL 60637, USA
[4]Max Planck Institute Florida, Jupiter, FL 33458, USA
[5]Neuroscience Research Unit, Pfizer Worldwide Research and Development, Cambridge, MA 02139, USA
[6]Department of Molecular and Human Genetics, Baylor College of Medicine, Houston, TX 77030, USA
*Correspondence: fan.wang@duke.edu
http://dx.doi.org/10.1016/j.neuron.2012.11.010

SUMMARY

Rodents begin to use bilaterally coordinated, rhythmic sweeping of their vibrissae ("whisking") for environmental exploration around 2 weeks after birth. Whether (and how) the vibrissal control circuitry changes after birth is unknown, and the relevant premotor circuitry remains poorly characterized. Using a modified rabies virus transsynaptic tracing strategy, we labeled neurons synapsing directly onto vibrissa facial motor neurons (vFMNs). Sources of potential excitatory, inhibitory, and modulatory vFMN premotor neurons, and differences between the premotor circuitry for vFMNs innervating intrinsic versus extrinsic vibrissal muscles were systematically characterized. The emergence of whisking is accompanied by the addition of new sets of bilateral excitatory inputs to vFMNs from neurons in the lateral paragigantocellularis (LPGi). Furthermore, descending axons from the motor cortex directly innervate LPGi premotor neurons. Thus, neural modules that are well suited to facilitate the bilateral coordination and cortical control of whisking are added to the premotor circuitry in parallel with the emergence of this exploratory behavior.

INTRODUCTION

Human infants acquire and refine controlled movements gradually, perhaps most conspicuously as they gain the ability to walk (Dominici et al., 2011; Gerber et al., 2010). An emerging idea is that these behavioral changes reflect the addition of new inputs from premotor control modules to lower-level motor control circuits, including motor neurons (Dominici et al., 2011). However, the identity of these added inputs is unknown and it is currently impractical to map them with high resolution in human subjects.

Rodents also acquire and refine movements during postnatal development, and they are amenable to high-resolution neural circuit tracing methods. One well-known example of a developmentally emergent behavior is exploratory whisking, the rhythmic sweeping movements of vibrissae (or whiskers) that rodents use to detect the texture, shape, and location of objects in their environment (Diamond et al., 2008; Kleinfeld et al., 2006). Whisking is usually bilaterally coordinated (Mitchinson et al., 2007; Sellien et al., 2005). Notably, although neonatal rodents can unilaterally retract their vibrissae as early as postnatal day 4 (P4), they only begin to exhibit bilateral whisking between P11 and P14 (Grant et al., 2012; Landers and Philip Zeigler, 2006; Welker, 1964; and our own observations in mouse), raising the possibility that this behavioral progression depends on changes to the central circuits that control vibrissal movements.

The final neural control of whisking is mediated by motor neurons in the lateral facial nucleus (FN), and these vibrissal facial motor neurons (vFMNs) form synapses with the intrinsic muscles surrounding the vibrissae or with the extrinsic muscles that extend throughout the mystacial pad (Ashwell and Watson, 1983; Dörfl, 1982; Hill et al., 2008; Wineski, 1985). Because vFMNs form neuromuscular junctions at late embryonic stages, and unilateral vibrissal movements are evident by P4 (Ashwell and Watson, 1983; Grant et al., 2012), the emergence of bilaterally coordinated whisking presumably involves the addition of new control inputs to the vFMNs as the animals mature. Furthermore, because whisking patterns and dynamics are regulated by the motor cortex (Berg et al., 2005; Berg and Kleinfeld, 2003; Brecht et al., 2004; Carvell et al., 1996; Donoghue and Parham, 1983; Hill et al., 2011; Li and Waters, 1991; Matyas et al., 2010), and both task-dependent whisking and vibrissae-dependent behaviors require the motor cortex (Huber et al., 2012), these added inputs must somehow link cortical signals to the vFMNs. In prior studies, investigators mapped neurons that project axons to or through the lateral FN in adult rodents using conventional retrograde tracing techniques (Hattox et al., 2002; Isokawa-Akesson and Komisaruk, 1987), but these

techniques could not selectively target neurons that synapse on vFMNs, nor could they reliably reveal how premotor inputs change during the critical early postnatal window when whisking first emerges.

To begin to address whether and how the vibrissal control circuitry changes over early postnatal life in the mouse, we employed a monosynaptic rabies-virus-based technique (Arenkiel and Ehlers, 2009; Callaway, 2008; Wickersham et al., 2007b) adapted to selectively trace neurons that directly synapse on the vFMNs (hereafter referred to collectively as the vFMN premotor circuitry). We mapped and compared the vFMN premotor circuitry before and immediately after the onset of whisking, and discovered that new modules are added to this circuitry in parallel with the emergence of the whisking behavior.

RESULTS

Mapping Premotor Inputs to vFMNs in Neonatal Mice prior to Whisking Onset

We sought to exploit monosynaptic viral tracing methods to selectively label neurons that make synapses onto vFMNs. Previous efforts led to the development of a glycoprotein-G-deleted mutant rabies virus (ΔG-RV) that cannot be transported into presynaptic neurons unless the infected source cell expresses rabies glycoprotein-G (rabies-G) to complement the mutant virus (Wickersham et al., 2007b). Once inside presynaptic neurons, which do not express rabies-G, the deficient virus ceases to spread further, and thus traces only neurons that are monosynaptically connected to the source cell (Wickersham et al., 2007b). To take advantage of this method for our study, we first generated a knockin mouse line at the *ROSA26* locus, where rabies-G is conditionally expressed in a Cre-dependent manner. Briefly, a ubiquitous CAG promoter followed by a loxp-neo-STOP-loxp cassette and a complementary DNA encoding rabies-G-IRES-TVA (i.e., CAG-loxp-STOP-loxp-rabies-G-IRES-TVA) was inserted into the intron of the *ROSA26* locus (Figure 1A; for the purpose of this study, TVA expression is irrelevant and thus will not be mentioned further). We refer to this new line as the RΦGT mouse, where Φ stands for the loxp-neo-STOP-loxp cassette.

We then confirmed that the RΦGT mouse does not facilitate leaky spreading of ΔG-RV particles in the absence of Cre transgene (Figures S2A–S2D). Specifically, injecting ΔG-RV-GFP (abbreviated as ΔG-GFP) into the mystacial pad in neonatal RΦGT mice resulted in infection and labeling of vFMNs, as well as some trigeminal sensory neurons that innervate vibrissa follicles and project axons into the brainstem, but did not label other cells in the CNS (Figures S2A–S2D). These experiments confirmed that in the absence of Cre, this approach labels only neurons that have axon terminals in the mystacial pad. We then crossed RΦGT mice with a transgenic mouse line that expresses Cre under the control of the choline-acetyl-transferase gene (Chat::Cre), allowing rabies-G to be expressed in all motor neurons, which are cholinergic and consequently can complement the deficient virus (Figure 1A). This double transgenic mouse allows for the selective labeling of vFMNs and their presynaptic partners following an injection of ΔG-RV into the mystacial pad (Figure 1A).

Using this approach, we first examined the vFMN premotor circuitry in neonatal Chat::Cre; RΦGT mice prior to the onset of whisking (<P11). Injection of ΔG-GFP into regions adjacent to the left B2 and C2 vibrissae in P1 pups (Figure 1B) led to infection of the intrinsic muscles that surround the B1-2 and C1-3 vibrissae, as well as small numbers of extrinsic muscle fibers between row B and row C (Figure 1B and data not shown). One week later (i.e., at P8), we sectioned and imaged each brain. As expected, labeled vFMNs were located in the lateral part of the FN (Figure 1D). These injections also resulted in a wide distribution of labeled cells spanning from the caudal medulla to the rostral brainstem (Movie S1, available online, scans through the entire set of serial coronal sections from a representative brain after P1→P8 transsynaptic tracing, giving an overview of the wide distributions of neurons presynaptic to vFMNs). A more detailed description is provided below and in Table S1.

Sensory-Related Inputs to vFMNs

We consistently observed labeled premotor neurons either within or adjacent to the three ipsilateral brainstem trigeminal nuclei that process sensory-related information from the vibrissae. In the most caudal part of the medulla, ΔG-GFP tracing labeled a group of neurons located in the dorsal medullary reticular formation (MdD) adjacent to the spinal caudalis (SpC) that extended radially oriented dendrites into the SpC (Figure 1E; Figure S1B). Within the rostral part of spinal interpolaris (SpIr), a group of neurons with large cell bodies and circumferentially oriented dendrites were labeled (Figures 1I–1J; Figure S1A). Furthermore, a cluster of smaller neurons adjacent to the spinal oralis (SpO) was traced by ΔG-GFP (Figure 1L; Figures S1A–S1B). Finally, GFP-labeled neurons, which presumably relay information about the head orientation onto vFMNs, were also found in the ipsilateral spinal vestibular nucleus (Ve; Figure 1I).

Medullary Reticular Inputs to vFMNs

GFP-labeled neurons were found in the intermediate reticular nuclei (IRt) and the gigantocellular reticular nuclei (Gi) both ipsilaterally and contralaterally, and in the midline raphe nuclei (Figures 1F–1H). In the IRt, numerous GFP-labeled neurons were located immediately adjacent to the nucleus ambiguus (NA; arrow in Figure 1F and arrowheads in Figure 1G; Figures S2I–S2L). Notably, extensive labeling was found in the pre-Bötzinger complex (preBötC) and Bötzinger complex (BötC; Figures 1I and 1K; Figures S1C–S1D), two regions that contain respiratory central pattern generator (CPG) neurons (Ezure, 1990; Smith et al., 1991, 2009). Although some respiratory CPG neurons are known to express somatostatin (*Sst*) and NK1R (Gray et al., 2001; Tan et al., 2008), most of the GFP-labeled premotor neurons in the preBötC area did not express *Sst* or NK1R (5% *Sst*+ and 8% NK1R+; Figures 2K and 2L; Table1).

Pontine and Midbrain Inputs to vFMNs

Scattered GFP-labeled cells were detected in the ventral pontine reticular formation (PnV; Movie S1). Dorsal to the principal trigeminal nucleus (PrV), we observed numerous GFP-labeled neurons in the Kölliker-Fuse (KF; Figure 1M), a region that is also known to regulate respiratory rhythms (Dutschmann and Herbert, 2006; Dutschmann et al., 2004). Finally, in the midbrain, GFP-labeled neurons were found in deeper layers of the superior colliculus (SC) and in the mesencephalic reticular nucleus (MRN; Figure 1N).

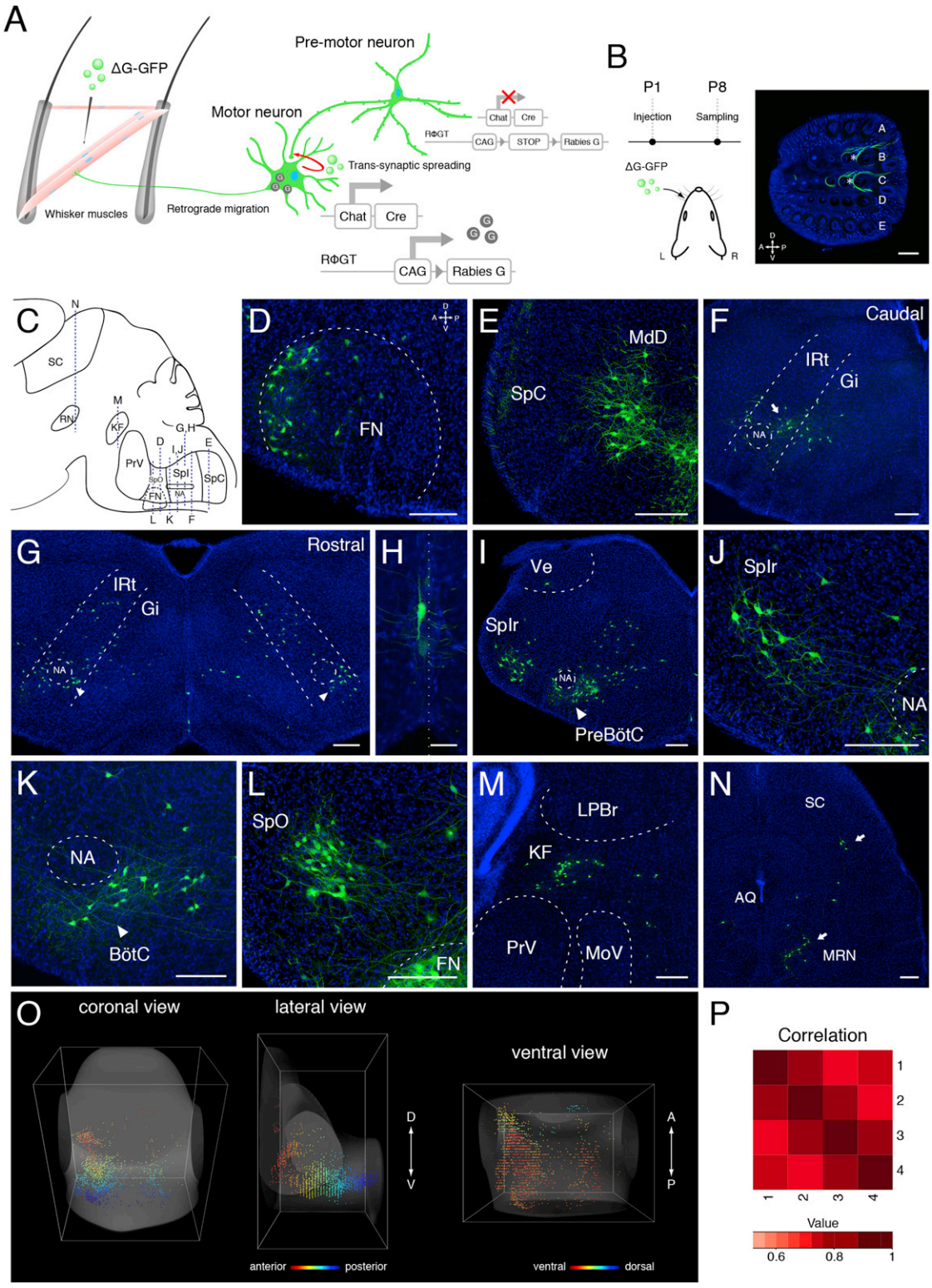

Figure 1. Monosynaptic Rabies-Virus-Mediated Transsynaptic Tracing of Vibrissa Premotor Neural Circuitry before the Onset of Active Whisking

(A) Schematic of the monosynaptic rabies virus tracing strategy used in this study.

(B) Left: Schematic representation of the time course of the experiment. Right: A tangential section of the left mystacial pad showing injection sites (stars), and labeled muscles around the injection sites. Letters indicate vibrissae rows. Scale bar, 500 μm.

(legend continued on next page)

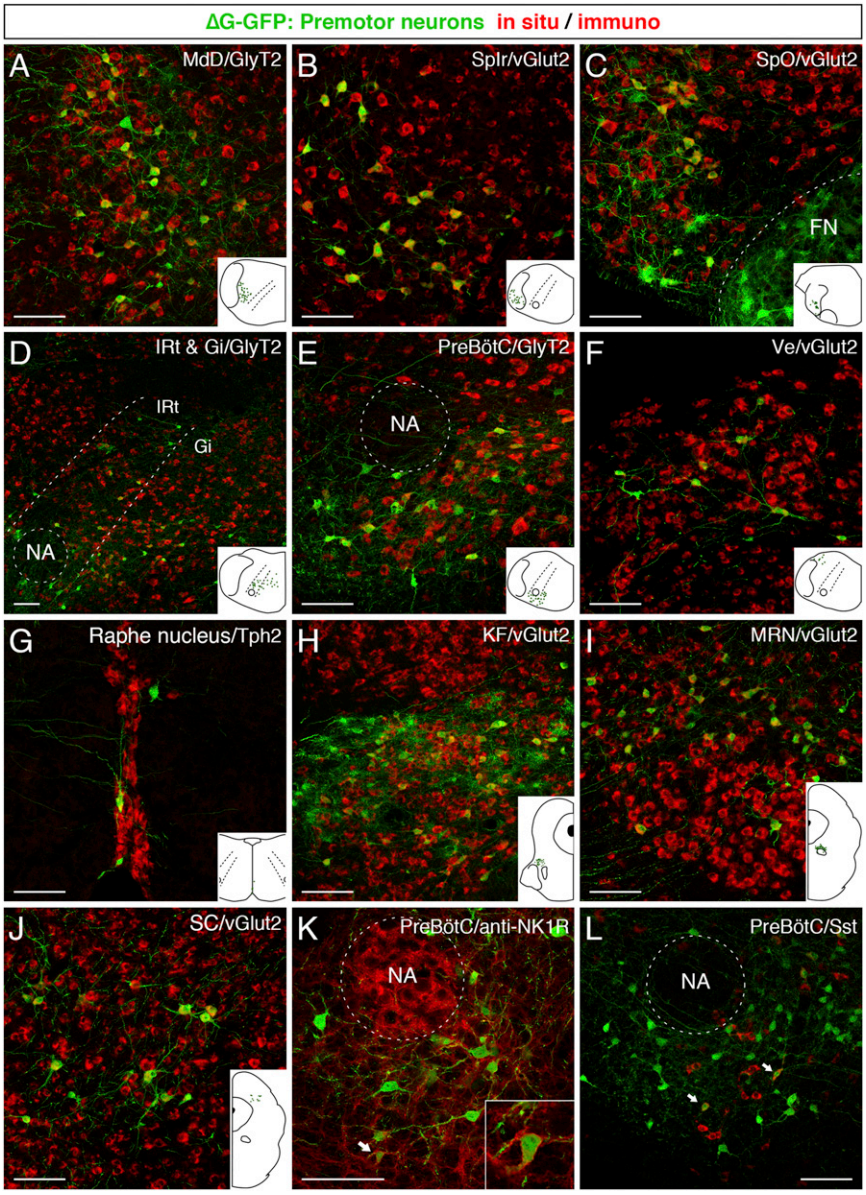

Figure 2. Neurotransmitter Phenotype Characterizations of vFMN Premotor Neurons

(A–J) Representative confocal images of ΔG-GFP (green) transsynaptically labeled brainstem sections hybridized with probes for *vGlut2*, *Gad1*, *Gad2*, *GlyT2*, and *Tph2* (red; P1 → P8 tracing). One selected marker is shown for each region of interest. See Figure S4 for additional markers. Anatomical locations of each image are indicated in the bottom-right corners. Scale bar, 100 μm. The results of this analysis are summarized in Table 1.

(K and L) Representative confocal images showing (K) NK1R (red, immunofluorescence) or (L) *Sst* (red, in situ) expressing neurons and virally labeled vFMN premotor neurons (green) located in the preBötC. Inset shows a high-magnification image of the neuron indicated by the arrow.

Scale bars, 100 μm.

See also Figure S4.

The numbers of GFP-labeled neurons in every structure containing vibrissa premotor neurons throughout the brainstem from four different animals are listed in Table S1. To measure the correlations of the transsynaptic tracing results among different animals, we aligned serial sections collected from each experimental brain and extracted each labeled neuron's spatial coordinates (see Experimental Procedures) to generate a three-dimensional (3D) reconstructed model of the transsynaptically traced circuitry for each animal (Figure 1O; Movie S2). A pairwise cross-correlation comparison (see Experimental Procedures) showed that the spatial distributions of the labeled premotor neurons were highly similar among the different animals (pairwise correlation coefficient r = 0.75–0.88; Figure 1P).

Further Validation of the Rabies Virus Transsynaptic Tracing Results

The consistent anatomical locations of GFP-labeled vFMN premotor neurons across different animals suggested to us that rabies-mediated monosynaptic circuit tracing is reproducible and therefore potentially suitable for discovering whether connectivity patterns change during development. We conducted two additional

(C) Sagittal illustration of the brainstem showing the approximate anterior-posterior positions of coronal sections shown in (D)–(N).

(D–N) Representative images of ΔG-GFP labeled neurons on coronal sections. Labeled neurons are observed in the lateral part of FN (D), in MdD adjacent to SpC (E), and in the caudal and rostral parts of IRt and Gi (F and G). Note that labeled neurons are enriched in regions surrounding the NA in the IRt (arrow in F and arrowheads in G). Labeled neurons are found bilaterally with an ipsilateral bias in the IRt and Gi. vFMN premotor neurons are also found in the raphe nucleus (dotted line denotes the midline, H), Ve (I), SpIr (I and J), preBötC (I), BötC (K), SpO (L), KF (M), deep layer of SC, and MRN (arrows, N). Scale bars, 200 μm (D–G and I–N) and 50 μm (H).

(O) 3D model of the brainstem showing the distribution of vFMN premotor neurons. Left: coronal view; middle: lateral view; right: ventral view. The dot colors denote rostrocaudal positions of vFMN premotor neurons in the 3D space.

(P) Cross-correlation analysis of distributions of vFMN premotor neurons from four animals. Color scale indicates correlation values (0.6–1).

See also Figures S1 and S3, Table S1, and Movies S1 and S2.

Table 1. Quantifications of In Situ Hybridization Analyses of vFMN Premotor Neurons

	Gad1/GFP (%)	*Gad2*/GFP (%)	*GlyT2*/GFP (%)	*vGlut2*/GFP (%)
MdD	9.36 ± 0.48	54.12 ± 1.26	84.26 ± 0.44	12.1 ± 0.65
PreBötC/BötC	30.36 ± 2.31	32.05 ± 1.19	34.84 ± 1.45	37.70 ± 0.73
IRt and Gi	16.12 ± 0.72	30.07 ± 1.54	37.36 ± 0.72	33.72 ± 2.52
Vestibular nucleus	33.33 ± 0	39.81 ± 5.78	39.49 ± 0.89	57.59 ± 2.09
SpIr	0	0	0	100 ± 0
SpO	3.51 ± 0.07	4.81 ± 0.71	11.16 ± 0.76	81.97 ± 0.63
Kölliker-Fuse	0	14.89 ± 0.85	0	82.26 ± 1.46
MRN	0	0	0	100 ± 0
Superior colliculus	0	0	0	100 ± 0
	Tph2/GFP (%)			*Sst*/GFP (%)
Raphe nucleus	28.42 ± 0.52		PreBötC/BötC	5.62 ± 1.31

Values represent the average (±SEM) percentages of neurons expressing the molecular markers per total GFP+ neurons in each of the indicated regions. Serial coronal sections from three ΔG-GFP virus-injected animals were analyzed for each marker. It is known that inhibitory neurons may co-express any combinations of *Gad1*, *Gad2*, and *GlyT2*. Thus, in some regions, the total percentage of *Gad1*+, *Gad2*+, *GlyT2*+, and *vGlut2*+ neurons may exceed 100% due to coexpression of markers.

experiments to better confirm this impression, as described below.

Examining the Possibility of Secondary Viral Spreading

Because the Chat::Cre driver results in expression of rabies-G also in all neurons that transiently or persistently express Chat (i.e., all central cholinergic neurons), it was important to determine that vFMNs were the only ΔG-GFP-labeled neurons derived from a Chat::Cre lineage in our experiments. We therefore performed ΔG-GFP transsynaptic tracing in triple transgenic Chat::Cre; RΦGT; RosaΦtomato mice. In these mice, RosaΦtomato (Arenkiel et al., 2011) serves as a red-fluorescence reporter for all cells that transiently or persistently express Chat::Cre activity. Importantly, no premotor neurons were double labeled with GFP and tomato, even though subsets of GFP-labeled neurons were located in close proximity to tomato-positive cells in many regions (Figures S2I–S2P). These results indicate that none of the premotor neurons we observed following ΔG-GFP injections in the mystacial pad were derived from a cholinergic lineage, and confirmed that no secondary spreading into pre-premotor neurons occurred under our experimental conditions.

Secondary Method to Further Substantiate the Monosynaptic Rabies Tracing Result

Because the deficient rabies virus is an excellent retrograde tracer that can infect wild-type neurons from their axons but cannot subsequently jump synapses without complementation (Etessami et al., 2000; Wickersham et al., 2007a), we also used ΔG-GFP as a conventional retrograde tracer to label inputs to the FN in wild-type neonatal mice. Injections of ΔG-GFP were made directly into the left lateral FN in wild-type pups at P6 (n = 4) and the distributions of labeled cells were analyzed at P9. In principle, such direct injections should label not only those neurons that synapse with vFMNs but also those with axons that extend through the injection site. Indeed, results from the direct retrograde tracing encompassed all locations uncovered by the transsynaptic tracing (Figure S3) and also resulted in GFP labeling at additional locations. These additional loci included the parvocellular reticular nucleus (PCRt), solitary nucleus (Sol), periaqueductal gray (PAG), and regions adjacent to the trigeminal motor nucleus (Figures S3B, S3D, and S3F). There was also significantly more labeling throughout the IRt and Gi, and midline raphe nucleus (Figures S3B–S3D). The numbers of all labeled neurons in all locations from four independently injected animals were counted and are listed in Table S1.

Neurotransmitter Phenotypes of vFMN Premotor Neurons

To identify the potential functional nature of inputs onto vFMNs from different sources, we used in situ hybridization to examine the expression of molecular markers for glutamatergic (*vGlut2*), GABAergic (*Gad1* and *Gad2*), glycinergic (*GlyT2*), or serotonergic (*Tph2*) transmission in GFP-labeled premotor neurons. Each of the four probes was hybridized to the entire serial sections of three different ΔG-GFP traced brains (n = 3 animals per probe, P1→P8 transsynaptic tracing from the mystacial pad). Figures 2A–2J show the representative images of one selected in situ probe together with GFP expression in each of the nuclei traced by ΔG-GFP (results of the other three probes for each region are shown in Figures S4A–S4O). Detailed quantitative results for the average percentage of marker-expressing cells among GFP-labeled neurons for each premotor structure are summarized in Table 1. Briefly, among the three pools of sensory-related premotor neurons, those located in the SpO and SpIr are mostly glutamatergic (*vGlut2*+), whereas those located in the MdD near SpC are primarily glycinergic (*GlyT2*+), and many of these also likely coexpress GABAergic markers (*Gad1/2*+). Premotor neurons in the various reticular nuclei (IRt, Gi, preBötC, and BötC) and in Ve are mixtures of *vGlut2*+, *GlyT2*+, and *Gad1/2*+ cells. Additionally, most of the GFP-labeled neurons in midline raphe nuclei (>70%) were labeled with markers for GABAergic transmission (*Gad1/2*+), whereas the remainder (28%) expressed serotonergic (*Tph2*+) markers. Finally, GFP-labeled cells rostral to

the FN from pons and midbrain, including those located in the KF, SC, and MRN, primarily expressed glutamatergic markers (*vGlut2*+; Table 1).

Differences in Premotor Pools Associated with Extrinsic Versus Intrinsic Muscles of the Mystacial Pad

We further explored whether we could use this modified rabies transsynaptic tracing method to identify differences in the premotor circuitry associated with vibrissa retraction versus protraction in neonatal mice. vFMNs that innervate the intrinsic muscles (vFMNs-in) are responsible for vibrissa protraction and project to the mystacial pad mostly through the buccal branch of the facial nerve, whereas those that innervate the caudal extrinsic muscle nasolabialis (vFMNs-ex) are partly responsible for vibrissa retraction and course through the zygomatic facial nerve (Dörfl, 1985; Hill et al., 2008; Klein and Rhoades, 1985; Figure 3A). Therefore, cutting the zygomatic nerve prior to ΔG-GFP injection into the mystacial pad should enable transsynaptic tracing primarily from vFMNs-in (Figure 3A, left). In contrast, injecting ΔG-GFP into the caudal nasolabialis muscle should selectively label subsets of vFMNs-ex and their associated inputs in Chat::Cre; RΦGT pups (P1→P8 tracing; Figure 3A, right).

An examination of the FN confirmed the relatively selective targeting of different vFMN subpopulations after such manipulations. Following viral injections into the caudal nasolabialis muscle, GFP-labeled neurons were found in the dorsolateral part of the FN (Figure 3C), whereas following injections near the vibrissae after zygomatic nerve transections, they were located in the lateral and ventrolateral part of the FN (Figure 3B). These localizations are in close agreement with previous studies that showed the relative positions of vFMNs-ex and vFMNs-in (Klein and Rhoades, 1985; Semba and Egger, 1986). The number of labeled vFMNs-ex (average 85 per animal) was about half that of labeled vFMNs-in (average 172 per animal). A comparison of the viral tracing results for vFMNs-in (n = 4) and vFMNs-ex (n = 4) revealed that the overall spatial distributions of premotor neurons for both groups of vFMNs were very similar (Figure 3).

Notably, we observed three differences in the pattern of premotor pools in the two vFMN subpopulations. First, significantly fewer neurons were labeled in the IRt when traced from vFMNs-ex (arrows in Figures 3F and 3G; when the number of labeled cells was divided by the number of infected vFMNs, the results were 0.65 ± 0.08 labeled IRt cells per vFMN-in, versus 0.34 ± 0.11 per vFMN-ex, $p < 0.03$). Second, markedly more neurons were labeled in the SpIr when traced from vFMNs-ex (Figures 3H–3K; 0.14 ± 0.08 SpIr neurons per vFMN-in, versus 1.79 ± 0.21 SpIr neurons per vFMN-ex, $p < 0.01$). Third, we did not observe any GFP-labeled neurons in the Ve when traced from intrinsic muscles, whereas they were consistently labeled from extrinsic muscles (arrows in Figures 3H and 3I). The latter finding suggests that vestibular derived sensory information feeds exclusively onto vFMNs-ex that control vibrissa retraction. This is consistent with the observation that horizontal rotations of the head are accompanied by ipsilateral vibrissa retraction in the direction of head turning, and the finding that rodents are capable of such unilateral vibrissal movements as early as P4 (Grant et al., 2012; Towal and Hartmann, 2006).

New Premotor Inputs to vFMNs Are Detected with the Emergence of Whisking

To map the vFMN premotor circuitry near the time in development when whisking is first observed (P11–P14; Grant et al., 2012; Landers and Philip Zeigler, 2006; Welker, 1964; and our observations in mouse), we injected ΔG-GFP at P8 in Chat::Cre; RΦGT mice and analyzed the resulting distribution of GFP-labeled cells at P15 (Figure 4A). Qualitatively, the infection efficiency of vFMNs from mystacial pad injection at P8 was lower than that seen with similar injections made at P1, and most of the infected vFMNs from such mystacial pad injections were vFMNs innervating intrinsic muscles (i.e., vFMNs-in), as judged by their positions in the ventrolateral FN (Figure 4F). Further, the vFMNs were highly susceptible to virus-induced pathology at this stage, as evidenced by the presumed clearance of dead vFMNs by infiltrating glial cells at 7 days postinfection (Figure 4F, stars). Nonetheless, the spatial distributions of labeled premotor neurons were still highly correlated among different animals at this stage (correlation coefficient r = 0.71–0.85; Figures 4H–4I). Movie S3 shows an entire series of sections through the brainstem from such P8→P15 tracing, Movie S4 is the 3D model showing the distribution of premotor neurons, and Table S2 lists the numbers of labeled neurons in different brainstem structures from four different animals.

Given the reduced efficacy of GFP labeling following ΔG-GFP injections made at P8, we focused our comparison with P1→P8 results on the locations of GFP-labeled premotor neurons rather than on their absolute numbers. Most P8→P15-labeled premotor neurons were found in the same nuclei as those observed before the onset of whisking (compare Movies S1 and S2 with Movies S3 and S4). For example, at both ages we found GFP-labeled neurons in the MdD (Movie S3); IRt and Gi (Figures S5A and S5B); preBötC, BötC, and KF (Figures 4B–4D); SpO (Figure S5C); ventral pons (Figure S5D); and SC and MRN (Movies S3 and S4). Furthermore, after the virus was injected selectively into the extrinsic nasolabialis muscles, we also found labeled cells in the SpIr and Ve, as observed following injections made earlier in development (Figures S5E and S5F).

Notably, P8→P15 transsynaptic tracing with unilateral injections of ΔG-GFP in the mystacial pad labeled a new group of neurons in the rostral part of the lateral paragigantocellularis (LPGi) both ipsilateral and contralateral to the injection site (arrows in Figure 4F, high magnification shown in Figure 4G; also see Movie S3). This group of neurons was never labeled in P1→P8 transsynaptic tracing (Figure 4E), despite the fact that P1-injected viruses infected significantly more vFMNs and premotor neurons than did P8-injected viruses. Moreover, injecting ΔG-RV into the extrinsic nasolabialis muscle in P8 mice after transecting the buccal nerve to prevent infection of vFMNs-in also labeled neurons in LPGi, although these labeled cells localized to a slightly more caudal position (Figures 4J–4L). Thus, both vFMNs-in and vFMNs-ex receive new sets of synaptic inputs from LPGi neurons around the time when the whisking behavior first emerges.

To further confirm the P8→P15 transsynaptic tracing results, we injected ΔG-GFP virus directly into the lateral FN at P12 and analyzed the brains at P15. Results from the direct retrograde tracing were highly variable but included all anatomical loci

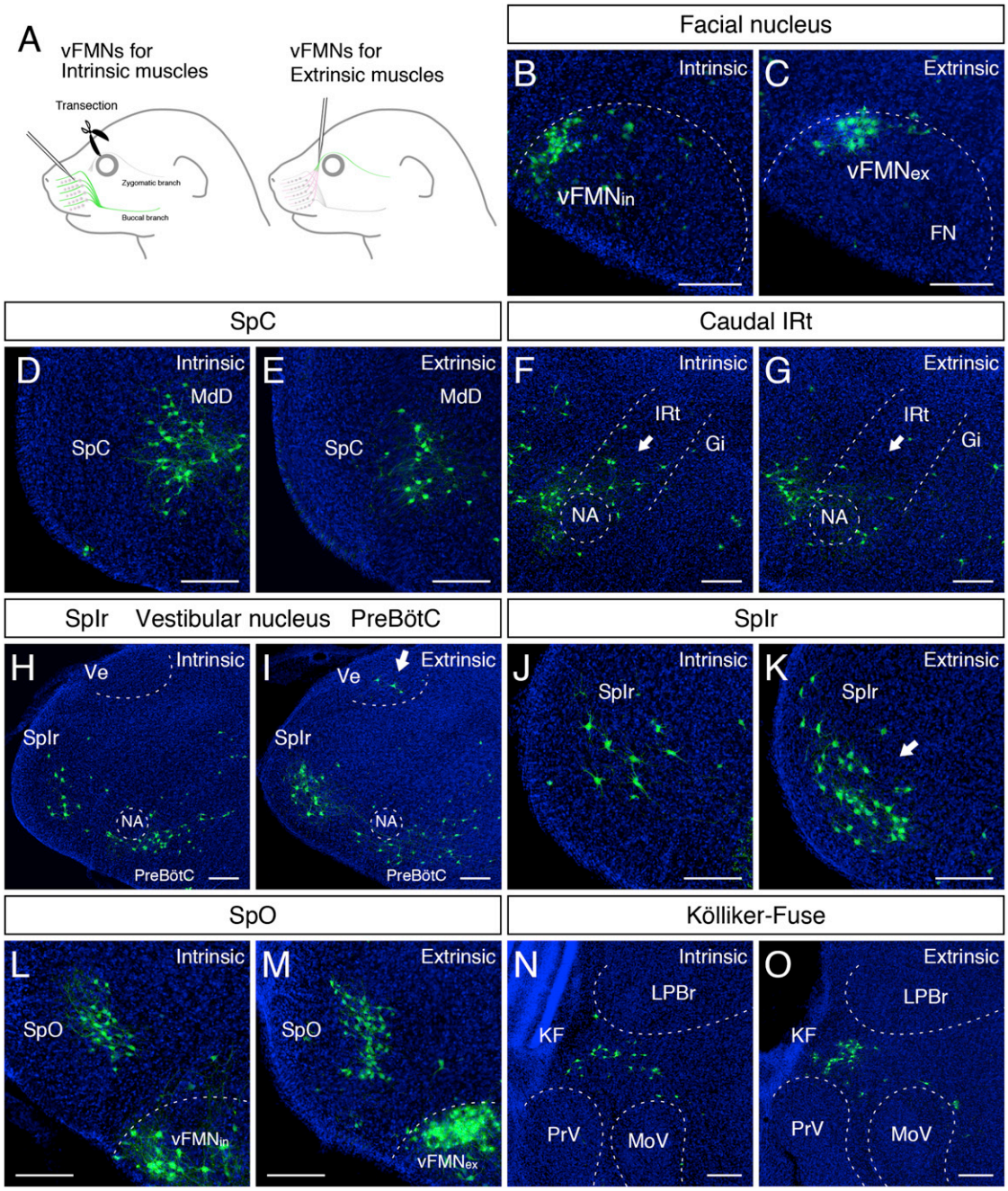

Figure 3. Premotor Inputs for vFMNs Innervating Intrinsic versus Extrinsic Muscles

(A) Left: Strategy to selectively label vFMN-in premotor neurons. Right: Strategy to selectively label vFMN-ex premotor neurons.

(B) ΔG-GFP-labeled vFMN-in located in the lateral and ventrolateral part of the FN.

(C) ΔG-GFP-labeled vFMN-ex located in the dorsolateral part of the FN.

(D–O) Comparisons of the distribution patterns between vFMN-in versus vFMN-ex premotor neurons in different brainstem nuclei. Similar labeling patterns are observed in the MdD (D and E), preBötC (H and I), BötC (data not shown), SpO (L and M), and KF (N and O). On the other hand, there are significantly more vFMN-in premotor neurons than vFMN-ex premotor neurons in the IRt adjacent to NA (arrows in F and G). In the Ve, vFMN premotor neurons are only observed following vFMN-ex tracing (H and arrow in I). In the SpIr, the number of labeled vFMN-ex premotor neurons is significantly higher than that of vFMN-in premotor neurons (J and arrow in K). Scale bar, 200 μm.

identified by transsynaptic tracing (Figure S6; Table S2). In addition, direct injection of virus into FN also labeled neurons in the PCRt, Sol, PAG, and regions adjacent to the trigeminal motor nucleus (Figures S6B–S6D and S6F; Table S2); all of these additional loci were similarly labeled in the P6→P9 direct FN infection experiments (Figure S3; Table S1).

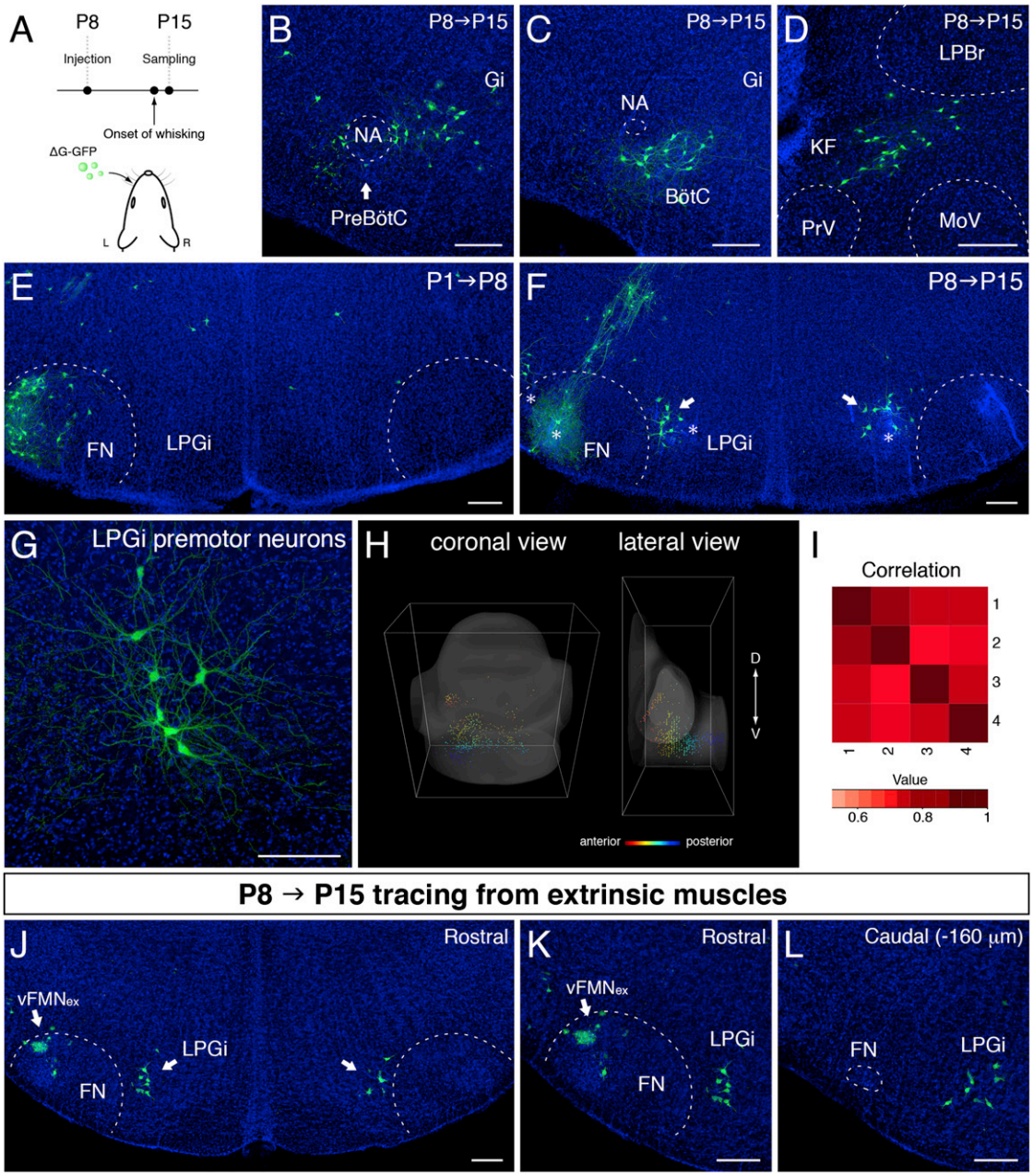

Figure 4. Monosynaptic Rabies-Virus-Mediated Transsynaptic Tracing of Vibrissa Premotor Neural Circuitry after the Onset of Active Whisking

(A) Schematic of the experimental strategy.

(B–D) Representative images of ΔG-GFP labeled vFMN premotor neurons from P8→P15 tracing in the respiration-related nuclei: preBötC (B), BötC (C), and KF (D). See Figure S5 for tracing results in other nuclei.

(E) No vFMN premotor neurons were found in LPGi following P1→P8 tracing.

(F) The new group of vFMN premotor neurons was found bilaterally in rostral LPGi following P8→P15 tracing (arrows). Stars indicate neuronal degeneration and glial infiltration (numerous DAPI-positive nuclei) in FN and LPGi.

(G) High-magnification image of LPGi premotor neurons.

(H) 3D model showing the distribution of vFMN premotor neurons after the onset of whisking. Left: coronal view; right: lateral view. The dot colors denote rostrocaudal positions of premotor neurons.

(I) Cross-correlation analysis of distributions of vFMN premotor neurons from four animals. Color scale indicates correlation values (0.6–1).

(J–L) vFMN-ex also receive new premotor inputs from neurons located in LPGi. (L) is 160 μm caudal to (K).

Scale bars, 200 μm (B–F and J–L) and 50 μm (G).

See also Figure S6, Table S2, and Movies S3 and S4.

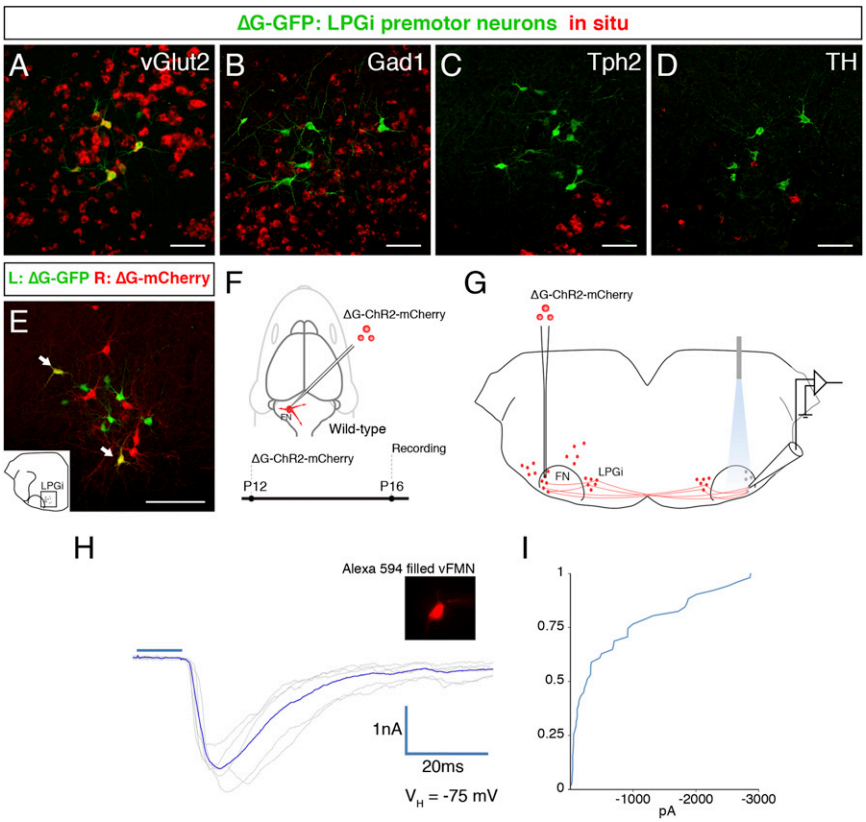

Figure 5. LPGi Premotor Neurons Are Glutamatergic, Project Bilaterally, and Provide Strong Monosynaptic Inputs to vFMNs

(A–D) In situ hybridization of coronal sections with probes for *vGlut2* (A), *Gad1* (B), *Tph2* (C), and TH (D, red). LPGi premotor neurons were visualized with anti-GFP (green). Scale bar, 100 μm.

(E) A representative image of the LPGi from P15 animals that received two-color virus injection at P8 (left; ΔG-GFP, right; ΔG-mCherry). Yellow indicates GFP- and mCherry-double-labeled neurons (arrows). Scale bar, 200 μm.

(F–I) Optogenetic examination of monosynaptic connectivity between LPGi neurons and vFMNs. (F) Schematic of the ΔG-ChR2-mCherry virus injection site and time course of the experiment. (G) Schematic of the recording strategy. ΔG-ChR2-mCherry virus retrogradely labels LPGi premotor neurons projecting bilaterally to FN. Recordings were made from the contralateral uninjected vFMNs. Focal illumination was targeted to ChR2-expressing axons in the contralateral FN. (H) Representative traces of whole-cell voltage-clamp recording from a contralateral vFMN in the presence of TTX and 4-AP. Light stimulus (10 ms duration) is indicated by the blue bar. The holding potential V_H is −75 mV. Inset shows an Alexa Fluor 594-filled vFMN. (I) Shows the cumulative probability distribution of response amplitude to optogenetic stimulation.

LPGi Neurons Are Glutamatergic and Make Bilateral Inputs onto vFMNs

What might be the synaptic function of these newly added LPGi premotor neurons on vFMNs? Using two-color in situ immunocolocalization methods, we found that GFP-labeled LPGi neurons express *vGlut2* (Figure 5A) but not *Gad1* (a GABAergic marker; Figure 5B), *Tph2* (a marker for serotonergic neurons; Figure 5C), or tyrosine hydroxylase (TH; Figure 5D), and therefore likely form glutamatergic synapses onto vFMNs. Because unilateral virus injections labeled neurons in both the left and right LPGi (Figures 4F and 4J), we wondered whether individual LPGi neurons project bilaterally to vFMNs. Following injections of ΔG-GFP and ΔG-mCherry into the left and right mystacial pads, respectively, we found that many LPGi neurons were double labeled, indicating that individual LPGi neurons innervate vFMNs bilaterally (Figure 5E). Importantly, no other double-labeled cells were found in our dual-color tracing experiments, strongly suggesting that LPGi neurons are likely to play an especially important role in coordinating vFMN activity bilaterally.

We used optogenetics-assisted electrophysiological recording methods (Petreanu et al., 2007, 2009) in brainstem slices to further characterize the functional nature of the synapses that LPGi axons make on vFMNs. To that end, we injected deficient rabies expressing channelrhodopsin and mCherry (ΔG-ChR2-mcherry; Osakada et al., 2011) into the left lateral FN to retrogradely infect LPGi premotor neurons on both sides of the brainstem (Figures 5F and 5G). Because many LPGi neurons project bilaterally, ΔG-ChR2-labeled LPGi neurons also send axons to the FN contralateral to the injection site. Thus, focal illumination of the contralateral FN with blue light should activate ChR2 on the axon terminals of LPGi neurons and trigger neurotransmitter release (Figure 5G). Using this strategy, we performed whole-cell voltage-clamp (V_H = −75 mV) recordings from randomly selected putative vFMNs (i.e., neurons located in the lateralmost part of the FN) contralateral to the injection site (Figure 5G). Brief (10 ms) illumination in the presence of tetrodotoxin (TTX) and 4-aminopyridine (4-AP) evoked large, fast, inward synaptic currents in half of the recorded vFMNs (five out of ten; Figures 5H and 5I). Because ΔG-ChR2 likely infects only subsets of LPGi neurons (that innervate subsets of vFMNs), we did not expect all randomly recorded vFMNs to respond to photostimulation. These findings indicate that LPGi neurons provide robust excitatory synaptic inputs onto vFMNs, which along with their bilateral projection patterns could enable them to drive bilaterally synchronized whisking.

LPGi Premotor Neurons Receive Excitatory Inputs from the Motor Cortex

It is known that exploratory whisking movements can be elicited and/or are modulated by cortical activity (Berg et al., 2005; Berg and Kleinfeld, 2003; Brecht et al., 2004; Carvell et al., 1996; Donoghue and Parham, 1983; Hill et al., 2011; Li and Waters, 1991; Matyas et al., 2010). A recent study in mice further showed that task-related whisking behavior depends on the motor cortex

(Huber et al., 2012). However, the vFMNs themselves receive only sparse synaptic inputs from the motor cortical axons (Grinevich et al., 2005). Therefore, we wondered whether transsynaptically labeled LPGi neurons are direct targets of cortical neurons, an arrangement that could enable descending signals from the motor cortex to affect vFMN activity and thus initiate and modulate the whisking behavior. To test this idea, we injected AAV-expressing GFP (AAV-GFP) into the right vibrissa motor cortex (M1) and then performed transsynaptic tracing by injecting ΔG-mCherry into the left B2/C2 vibrissae at P8 (Figure 6A). We found that GFP-labeled collaterals of the motor cortical axons traversed through regions where mCherry-labeled LPGi premotor neurons were located (Figures 6B–6D). We used anti-vGlut1 to stain presynaptic terminals and found that the motor cortical axons appeared to make numerous synapses onto LPGi premotor neurons (Figures 6D–6G). Similarly, AAV-GFP viruses injected into the primary somatosensory cortex (S1; Figure 6A) also labeled axon collaterals coursing through the LPGi region (Figure 6H). However, S1 axons appeared to form sparser vGlut1+ terminals on LPGi neurons (Figures 6I and 6J). We counted the numbers of putative motor or somatosensory cortical synapses (i.e., vGlut1+ boutons) on every transsynaptically labeled LPGi neuron (n = 3 different animals for each case). On average, the M1 axons formed twice as many vGlut1+ boutons on LPGi neurons than did the S1 axons (Figure 6K).

To ascertain the functions of these putative cortical synapses on LPGi neurons, we obtained whole-cell voltage-clamp recordings from ΔG-mCherry transsynaptically labeled LPGi neurons while activating motor cortical inputs using optogenetic methods (Petreanu et al., 2007, 2009). First, AAV-Channelrhodopsin (AAV-ChR2) was injected into M1 at P2 (Figure 6L). ΔG-mCherry was then injected into the vibrissae at P8, and coronal brainstem slices were prepared at P14 (Figures 6L and 6M). Focal illumination of ChR2-expressing cortical axons in LPGi in the presence of TTX and 4-AP evoked fast, inward synaptic currents in seven out of 25 transsynaptically labeled LPGi neurons (V_H = −75 mV; Figures 6N and 6O), consistent with the notion that motor cortical axons make excitatory synapses on LPGi neurons. Taken together, these results indicate that LPGi neurons are in a key position to relay motor cortical signals bilaterally to vFMNs.

DISCUSSION

Here, we used monosynaptic rabies-virus-based tracing, in situ molecular analysis of virally labeled neurons, and optogenetics-assisted electrophysiological recordings to map and functionally characterize the premotor circuitry for vibrissal control in the neonatal mouse before and after a critical developmental landmark, namely the emergence of whisking behavior. We further assigned putative functions to vibrissal premotor inputs by using in situ hybridization to assess the neurotransmitter phenotypes of virally labeled premotor neurons. The premotor wiring diagram with transmitter signs is summarized in Figure 7. In parallel with the developmental onset of whisking, we detected the addition of a new premotor module that is well suited to bilaterally coordinate and potentially synchronize vibrissal movements and facilitate cortical modulation of whisking, which are two characteristic features of this exploratory behavior.

Our study selectively traces inputs to vFMNs during the first 2 weeks of postnatal life, when exploratory whisking first emerges. Although prior studies in adult rats used conventional retrograde tracers (i.e., horseradish peroxidase or cholera toxin B) to trace inputs to the lateral FN (Hattox et al., 2002; Isokawa-Akesson and Komisaruk, 1987), it is likely that injection of these tracers directly into the FN labeled not only inputs to vFMNs but also other neurons that either project axons through the injection site or make synapses with facial motor neurons other than vFMNs. In contrast, the transsynaptic tracing method used here allowed us to infect specific groups of vFMNs with monosynaptic rabies viruses and subsequently label their inputs more precisely. The different specificities of conventional methods likely explain why such approaches label a wider range of loci, including the PCRt, Sol, PAG, and peritrigeminal motor nucleus, than observed with the monosynaptic rabies method. In fact, these additional loci were also labeled when we injected ΔG-RV directly into the lateral FN, an approach that is likely to label other inputs to the FN besides those that terminate on vFMNs. Additionally, previous conventional tracing of inputs to the FN also labeled numerous neurons in the midbrain red nucleus (Hattox et al., 2002; Isokawa-Akesson and Komisaruk, 1987), which were not labeled in our transsynaptic tracing. A possible explanation for this discrepancy is that diffusion of tracer from the lateral FN may have spread into the juxtaposed rubrospinal tract, resulting in false-positive labeling of neurons in the red nucleus.

The monosynaptic rabies tracing method employed here is not without limitations. Although prior studies established that rabies virions produced from an infected neuron spread predominantly to its presynaptic partners (Kelly and Strick, 2000; Ugolini, 1995), at longer time points postinfection, virus particles that are shed by dying neurons may infect nearby axon terminals and glial cells (e.g., Figures S2G and S2H show labeled glial fibrillary acidic protein [GFAP]-positive glial cells in FN). Although we cannot entirely rule out the possibility of false-positive labeled neurons, we used relatively short survival times, and our transsynaptic tracing method labeled fewer loci than observed in other studies using conventional tracers, as described above. Furthermore, the LPGi premotor neurons are situated immediately outside the FN, and in fact, direct injection of ΔG-RV into lateral FN in P6→P9 retrograde tracing experiments labeled these neurons (Figure S3; Table S1), likely due to their proximity to FN. Had the virus leaked from dying neurons in our transsynaptic tracing experiment and infected nearby neurons, we would have also labeled LPGi neurons in our P1→P8 transsynaptic tracing, yet this did not happen. Instead, LPGi neurons were only labeled in P8→P15 transsynaptic tracing, arguing against nonsynaptic spreading. A second potential limitation is that the rabies virus jumps synapses in a stochastic fashion, and thus may fail to label neurons that make only very sparse inputs to the infected cell. This feature of the rabies tracing method could explain why we recovered only small numbers of labeled neurons in the cortex, and only when we injected larger volumes of the virus into multiple vibrissae (Figures S1E–S1H). Notwithstanding these limitations,

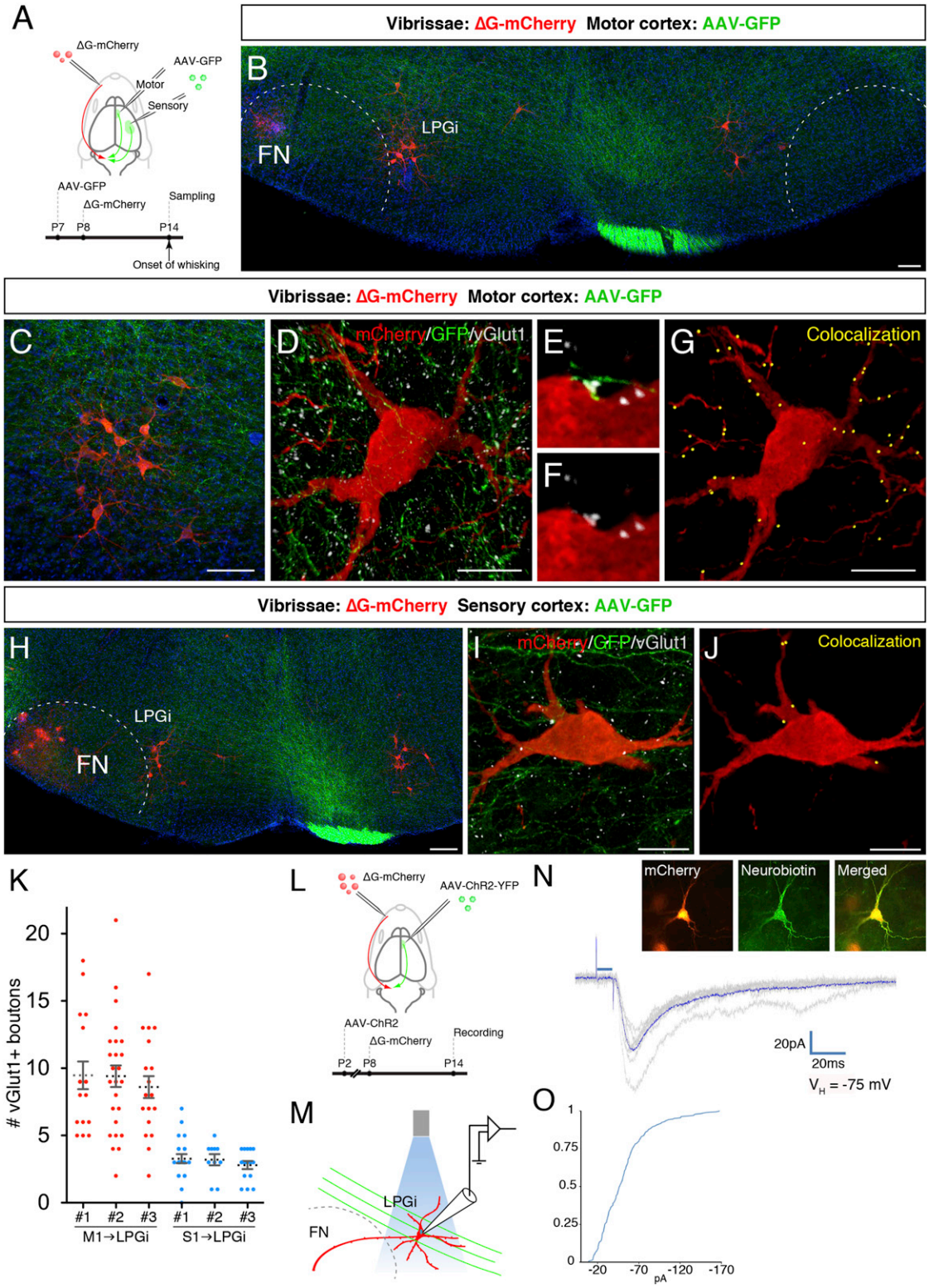

Figure 6. LPGi Premotor Neurons Receive Direct Motor Cortical Inputs

(A) Strategy to label cortical axons and LPGi premotor neurons. AAV-GFP was injected stereotaxically into the right primary motor (M1) or primary somatosensory cortex (S1) of Chat::Cre; RΦGT mice at P7. The animals then received ΔG-mCherry injection near the left B2/C2 vibrissa at P8 to transsynaptically label LPGi premotor neurons, and brains were collected at P14.

(legend continued on next page)

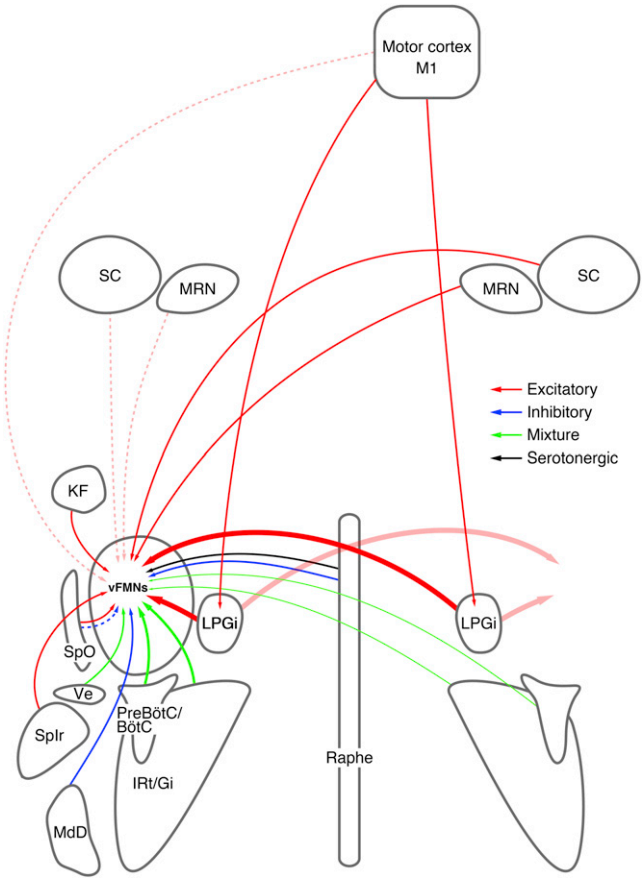

Figure 7. Wiring Diagram of the Premotor Circuitry for vFMNs
Thicker lines indicate LPGi inputs that are added at the onset of whisking. Dotted lines indicate sparse inputs. Neurotransmitter phenotypes are indicated by different colors (red, glutamatergic; blue, glycinergic and/or GABAergic; green, mixture of glutamatergic/GABAergic/glycinergic; black, serotonergic).

the monosynaptic rabies virus used here presents a useful strategy for selectively tracing inputs to motor neurons through intramuscular injections (Stepien et al., 2010), an approach that greatly simplifies mapping of premotor circuitry at early developmental stages when precise targeting of injections to brainstem motor nuclei can be challenging. Here, this approach enabled us to detect developmental changes in the vFMN premotor circuitry.

The in situ-GFP colocalization analysis performed here represents an initial step in characterizing the functional properties of the various synaptic inputs onto vFMNs (Figure 7; Table 1). For example, we found that GFP-labeled LPGi neurons express glutamatergic markers, and whole-cell recordings from vFMNs combined with optogenetic stimulation of LPGi axons showed that LPGi axon terminals can evoke robust, fast, inward synaptic currents in vFMNs, consistent with fast excitatory synaptic transmission involving ionotropic glutamate receptors. In contrast, a previous study showed that direct electrical stimulation in the LPGi region elicited vibrissal movements, and ascribed these behavioral effects to the actions of serotonin (5-HT) because of the presence of 5-HT fibers in LPGi and the observation that 5-HT application can elicit periodic firing in vFMNs (Hattox et al., 2003). The present findings suggest that the glutamatergic synapses formed by LPGi premotor neurons on vFMNs also contribute significantly to the vibrissal movements evoked by electrical stimulation of the LPGi. Although a full characterization of the functional nature of various components of the vFMN premotor circuitry is beyond the scope of this study, the transmitter phenotype analysis we performed here highlights the remarkable diversity of the synaptic inputs onto vFMNs.

The developmental addition of bilateral-projecting neurons in the LPGi to the vFMN premotor circuitry provides a plausible anatomical substrate for the emergence of whisking, which is characterized by cortically modulated, bilaterally coordinated movements of the vibrissae. When rodents whisk freely in air, vibrissae on both sides of the head move synchronously at similar amplitudes and frequencies (Gao et al., 2001; Sellien et al., 2005). Even when asymmetric bilateral vibrissal movements occur as a result of contact with objects on one side of the head or head turning, both sides usually continue to whisk at the same frequency and/or in phase, and hence are still bilaterally coordinated (except in object-localization tasks in head-fixed mice; Mitchinson et al., 2007; O'Connor et al., 2010; Sachdev et al., 2003; Towal and Hartmann, 2006). Electrophysiological recordings show that LPGi axons provide potent

(B–G) Anatomical examination of M1-LPGi connectivity. (B) Representative image showing M1 axons (green) coursing by LPGi neurons (red). Blue is DAPI. Scale bar, 200 μm. (C) High-magnification image of the LPGi region. Scale bar, 100 μm. (D–G) Representative images of three-color immunofluorescence showing LPGi premotor neurons (red), motor cortex axons (green) and presynaptic terminals (anti-vGlut1, white). (E and F) High-magnification images of a GFP+ motor cortical axon with a vGlut1+ terminal putatively synapsing onto an LPGi neuron. (G) GFP+/vGlut1+ M1 synaptic terminals on the LPGi neuron are represented as yellow dots. Scale bar, 20 μm.
(H–J) Anatomical examination of S1-LPGi connectivity. (H) Representative image showing S1 axons coursing through LPGi. Scale bar, 200 μm. (I) Representative confocal images of three-color immunofluorescence showing LPGi premotor neurons (red), S1 axons (green), and presynaptic terminals (anti-vGlut1, white). (J) GFP+/vGlut1+ S1 synaptic terminals on the LPGi neuron are represented as yellow dots. Scale bar, 20 μm.
(K) Quantification of vGlut1+ cortical presynaptic boutons on individual LPGi neurons (individual dots). M1 → LPGi (red dots, n = 3 mice), S1 → LPGi (blue dots, n = 3 mice). Error bars represent mean ± SEM.
(L–O) Optogenetic examination of monosynaptic connectivity between M1 and LPGi premotor neurons. (L) Schematic of the virus injection site and time course of the experiment. (M) Schematic of the recording strategy. Recordings were targeted to transsynaptically labeled LPGi neurons (red) with focal illumination of ChR2-expressing cortical axons in LPGi. (N) Representative traces of a whole-cell, voltage-clamp recording from a transsynaptically labeled LPGi neuron in the presence of TTX and 4-AP. Light stimulus (10 ms duration) is indicated by the blue bar. Holding potential V_H is −75 mV. Insets show a recorded LPGi neuron (red) filled with neurobiotin and stained with streptavidin Alexa Fluor 488 (green). (O) Cumulative probability distribution of response amplitude to optogenetic stimulation.

excitatory input bilaterally to vFMNs, suggesting that LPGi premotor neurons are well suited to synchronize and coordinate bilateral vFMN firing. Furthermore, cortical axons form numerous synapses on LPGi neurons, suggesting that LPGi premotor neurons are especially well positioned to relay cortical commands to vFMNs to facilitate cortical modulation of whisking patterns, kinematics, and behaviors (Berg et al., 2005; Berg and Kleinfeld, 2003; Brecht et al., 2004; Carvell et al., 1996; Donoghue and Parham, 1983; Hill et al., 2011; Huber et al., 2012; Li and Waters, 1991; Matyas et al., 2010).

The developmental addition of new premotor modules, as seen here for murine vibrissal circuitry, may be a general theme underlying the postnatal acquisition and refinement of behaviors in vertebrates. For example, juvenile zebra finches initially produce babbling-like subsongs, but abruptly begin to produce "plastic" songs with identifiable syllables and phrases near the end of the seventh week after hatching (Aronov et al., 2008; Immelman, 1969). This behavioral transition follows the formation of synaptic connections between the song premotor nucleus HVC and the song motor nucleus RA, suggesting that the emergence of plastic songs depends on the developmental addition of the HVC module to the premotor pathway (Aronov et al., 2008; Mooney, 1992; Mooney and Rao, 1994). Human infants also transition from infant stepping to toddler walking, from babbling to talking, and from grasping-like hand movements to fine finger movements (Gerber et al., 2010; Kuhl and Meltzoff, 1996; Wallace and Whishaw, 2003), and these behavioral changes likely require the addition of new control modules to the relevant motor pathways (Dominici et al., 2011). Therefore, development of the vertebrate nervous system may first involve the formation of neural circuitry for primitive movements, followed later by the addition of premotor modules that enable the generation of behaviors necessary for environmental and social exploration.

EXPERIMENTAL PROCEDURES

Mouse

RΦGT Mice

A CAG-loxp-neo-loxp-rabies-G-IRES-TVA cassette was inserted into the rosa26 locus to generate the RΦGT mice. The Chat::Cre mouse line was purchased from Jackson Laboratories (stock #006410). All Chat::Cre; RΦGT mice used in this study carry one Chat::Cre allele and one RΦGT allele (i.e., heterozygous for both alleles).

Virus Tracing Experiments

Chat::Cre

RΦGT mice were anesthetized by hypothermia (P1) or with ketamine/xylazine (50 mg/kg and 5 mg/kg, i.p.; P8) and injected with ΔG-mCherry or ΔG-GFP into the mystacial pad at P1 or P8, and brains were collected at 7 days postinfection. To selectively infect motor neurons innervating intrinsic muscles (vFMN-in), the zygomatic branch was first transected at the location anterior to the eye, followed by injection of ΔG-GFP virus into the mystacial pad. To selectively infect motor neurons innervating extrinsic muscles (vFMN-ex), ΔG-GFP was injected into the caudal end of the nasolabialis muscle just under the dermis. For direct retrograde tracing with ΔG-RV, ΔG-GFP was stereotaxically injected into the left side of the lateral FN of wild-type mice (C57/BL6) at P6 or P12, and brains were collected 3 days postinfection. For AAV2-GFP (University of Pennsylvania Vector Core) and ΔG-mCherry double-tracing experiments, AAV2-GFP was stereotaxically injected into the right side of the motor or somatosensory cortex at P7, and ΔG-mCherry was injected into the left mystacial pad as described above at P8.

Image Acquisition and Cross-Correlation Analysis of the 3D Spatial Distributions of Labeled Neurons

The x, y, z coordinates of labeled neurons from all serial sections were obtained using the IMARIS Spots function, and 3D models were reconstructed using IMARIS software.

To compare the spatial distribution of labeled neurons across individuals, the space covered by the 3D data points was evenly divided into identical-sized cubes. Dividing the brain into a range of cubes from 10×10×10 (1,000 cubes) to 50×50×50 (125,000 cubes) yields essentially identical cross-correlation coefficiencies between animal pairs. Specifically, the number of labeled neurons inside each cube was counted, and similarity between two mice was measured by the Pearson correlation coefficient. Standardization, correlation calculation, and heatmap plotting were performed using the statistical software R (http://www.r-project.org).

Immunostaining and in situ hybridization were performed according to standard procedures.

Optogenetics-Assisted Electrophysiological Recordings

To examine the motor cortex-LPGi connection, Chat::Cre; RΦGT mice were injected with AAV2-ChR2-YFP (University of Pennsylvania Vector Core) and ΔG-mCherry into the right side of the motor cortex at P2 and the left side of the mystacial pad at P8, respectively. Brainstem slices were prepared at P14. To examine the LPGi-vFMNs connection, ΔG-ChR2-mCherry (Osakada et al., 2011) was stereotaxically injected into the left side of the lateral FN of wild-type (C57BL/6) mice at P12. Recordings were performed from the contralateral (right side) uninjected FN.

Coronal brainstem slices were incubated for 14 min in a 34°C bath of carbogenated modified artificial cerebrospinal fluid (ACSF) containing (in mM) 92 *N*-methyl-D-glucamine, 2.5 KCl, 1.2 NaH_2PO_4, 30 $NaHCO_3$, 20 HEPES, 25 dextrose, 5 sodium ascorbate, 2 thiourea, 3 sodium pyruvate, 10 $MgSO_4$, 0.5 $CaCl_2$. All recordings were made in whole-cell, voltage-clamp configuration using a Multiclamp 700B amplifier, the output of which was digitized at 10 kHz (Digidata 1440A), and all recordings were made in room-temperature ACSF containing 1 μM TTX (Sigma) + 100 μM 4-AP (Tocris). ChR2-expressing axon terminals were stimulated with brief pulses (10 ms, though 2 ms pulses were sufficient) of 473 nm laser light (Shanghai Laser and Optics BL473T3-150) presented directly over the recording location with a 200 μm jacketed fiber optic (Thor Labs). See Supplemental Experimental Procedures for more details.

SUPPLEMENTAL INFORMATION

Supplemental Information includes six figures, two tables, four movies, and Supplemental Experimental Procedures and can be found with this article online at http://dx.doi.org/10.1016/j.neuron.2012.11.010.

ACKNOWLEDGMENTS

We thank Ed Callaway for providing various ΔG rabies viruses and Yingchun Ni and Zhigang He for help with producing viruses. We thank Bao-Xia Han for general technical support and members of the Wang laboratory and Mooney laboratory for discussions and suggestions. We thank Martin Deschenes, Jeff Moore, and David Kleinfeld for sharing results prior to publication. We thank Drs. Stephen Lisberger, Rebecca Yang, Martin Deschenes, Jeff Moore, and David Kleinfeld for critically reading the manuscript. This work was supported by NIH grants DA028302 and DE019440 to F.W., NS079929 to R.M., and NS078294 to B.R.A., who was also supported by the McNair Foundation. J.T. was supported in part by an incubator award from Duke Institute of Brain Sciences. Correspondence for the RΦGT (rosa26-CAG-loxP-STOP-loxP-rabies-G-TVA) mouse should be addressed to B.R.A. (arenkiel@bcm.edu).

Accepted: November 5, 2012
Published: January 23, 2012

REFERENCES

Arenkiel, B.R., and Ehlers, M.D. (2009). Molecular genetics and imaging technologies for circuit-based neuroanatomy. Nature *461*, 900–907.

Arenkiel, B.R., Hasegawa, H., Yi, J.J., Larsen, R.S., Wallace, M.L., Philpot, B.D., Wang, F., and Ehlers, M.D. (2011). Activity-induced remodeling of olfactory bulb microcircuits revealed by monosynaptic tracing. PLoS ONE *6*, e29423.

Aronov, D., Andalman, A.S., and Fee, M.S. (2008). A specialized forebrain circuit for vocal babbling in the juvenile songbird. Science *320*, 630–634.

Ashwell, K.W., and Watson, C.R. (1983). The development of facial motoneurones in the mouse—neuronal death and the innervation of the facial muscles. J. Embryol. Exp. Morphol. *77*, 117–141.

Berg, R.W., and Kleinfeld, D. (2003). Vibrissa movement elicited by rhythmic electrical microstimulation to motor cortex in the aroused rat mimics exploratory whisking. J. Neurophysiol. *90*, 2950–2963.

Berg, R.W., Friedman, B., Schroeder, L.F., and Kleinfeld, D. (2005). Activation of nucleus basalis facilitates cortical control of a brain stem motor program. J. Neurophysiol. *94*, 699–711.

Brecht, M., Krauss, A., Muhammad, S., Sinai-Esfahani, L., Bellanca, S., and Margrie, T.W. (2004). Organization of rat vibrissa motor cortex and adjacent areas according to cytoarchitectonics, microstimulation, and intracellular stimulation of identified cells. J. Comp. Neurol. *479*, 360–373.

Callaway, E.M. (2008). Transneuronal circuit tracing with neurotropic viruses. Curr. Opin. Neurobiol. *18*, 617–623.

Carvell, G.E., Miller, S.A., and Simons, D.J. (1996). The relationship of vibrissal motor cortex unit activity to whisking in the awake rat. Somatosens. Mot. Res. *13*, 115–127.

Diamond, M.E., von Heimendahl, M., Knutsen, P.M., Kleinfeld, D., and Ahissar, E. (2008). 'Where' and 'what' in the whisker sensorimotor system. Nat. Rev. Neurosci. *9*, 601–612.

Dominici, N., Ivanenko, Y.P., Cappellini, G., d'Avella, A., Mondì, V., Cicchese, M., Fabiano, A., Silei, T., Di Paolo, A., Giannini, C., et al. (2011). Locomotor primitives in newborn babies and their development. Science *334*, 997–999.

Donoghue, J.P., and Parham, C. (1983). Afferent connections of the lateral agranular field of the rat motor cortex. J. Comp. Neurol. *217*, 390–404.

Dörfl, J. (1982). The musculature of the mystacial vibrissae of the white mouse. J. Anat. *135*, 147–154.

Dörfl, J. (1985). The innervation of the mystacial region of the white mouse: A topographical study. J. Anat. *142*, 173–184.

Dutschmann, M., and Herbert, H. (2006). The Kölliker-Fuse nucleus gates the postinspiratory phase of the respiratory cycle to control inspiratory off-switch and upper airway resistance in rat. Eur. J. Neurosci. *24*, 1071–1084.

Dutschmann, M., Mörschel, M., Kron, M., and Herbert, H. (2004). Development of adaptive behaviour of the respiratory network: implications for the pontine Kolliker-Fuse nucleus. Respir. Physiol. Neurobiol. *143*, 155–165.

Etessami, R., Conzelmann, K.K., Fadai-Ghotbi, B., Natelson, B., Tsiang, H., and Ceccaldi, P.E. (2000). Spread and pathogenic characteristics of a G-deficient rabies virus recombinant: an in vitro and in vivo study. J. Gen. Virol. *81*, 2147–2153.

Ezure, K. (1990). Synaptic connections between medullary respiratory neurons and considerations on the genesis of respiratory rhythm. Prog. Neurobiol. *35*, 429–450.

Gao, P., Bermejo, R., and Zeigler, H.P. (2001). Whisker deafferentation and rodent whisking patterns: behavioral evidence for a central pattern generator. J. Neurosci. *21*, 5374–5380.

Gerber, R.J., Wilks, T., and Erdie-Lalena, C. (2010). Developmental milestones: motor development. Pediatr. Rev. *31*, 267–276, quiz 277.

Grant, R.A., Mitchinson, B., and Prescott, T.J. (2012). The development of whisker control in rats in relation to locomotion. Dev. Psychobiol. *54*, 151–168.

Gray, P.A., Janczewski, W.A., Mellen, N., McCrimmon, D.R., and Feldman, J.L. (2001). Normal breathing requires preBötzinger complex neurokinin-1 receptor-expressing neurons. Nat. Neurosci. *4*, 927–930.

Grinevich, V., Brecht, M., and Osten, P. (2005). Monosynaptic pathway from rat vibrissa motor cortex to facial motor neurons revealed by lentivirus-based axonal tracing. J. Neurosci. *25*, 8250–8258.

Hattox, A., Li, Y., and Keller, A. (2003). Serotonin regulates rhythmic whisking. Neuron *39*, 343–352.

Hattox, A.M., Priest, C.A., and Keller, A. (2002). Functional circuitry involved in the regulation of whisker movements. J. Comp. Neurol. *442*, 266–276.

Hill, D.N., Bermejo, R., Zeigler, H.P., and Kleinfeld, D. (2008). Biomechanics of the vibrissa motor plant in rat: rhythmic whisking consists of triphasic neuromuscular activity. J. Neurosci. *28*, 3438–3455.

Hill, D.N., Curtis, J.C., Moore, J.D., and Kleinfeld, D. (2011). Primary motor cortex reports efferent control of vibrissa motion on multiple timescales. Neuron *72*, 344–356.

Huber, D., Gutnisky, D.A., Peron, S., O'Connor, D.H., Wiegert, J.S., Tian, L., Oertner, T.G., Looger, L.L., and Svoboda, K. (2012). Multiple dynamic representations in the motor cortex during sensorimotor learning. Nature *484*, 473–478.

Immelman, K. (1969). Song development in the zebra finch and other estrildid finches. In Bird Vocalizations, R.A. Hinde, ed. (Cambridge, UK: Cambridge University Press), pp. 61–77.

Isokawa-Akesson, M., and Komisaruk, B.R. (1987). Difference in projections to the lateral and medial facial nucleus: anatomically separate pathways for rhythmical vibrissa movement in rats. Exp. Brain Res. *65*, 385–398.

Kelly, R.M., and Strick, P.L. (2000). Rabies as a transneuronal tracer of circuits in the central nervous system. J. Neurosci. Methods *103*, 63–71.

Klein, B.G., and Rhoades, R.W. (1985). Representation of whisker follicle intrinsic musculature in the facial motor nucleus of the rat. J. Comp. Neurol. *232*, 55–69.

Kleinfeld, D., Ahissar, E., and Diamond, M.E. (2006). Active sensation: insights from the rodent vibrissa sensorimotor system. Curr. Opin. Neurobiol. *16*, 435–444.

Kuhl, P.K., and Meltzoff, A.N. (1996). Infant vocalizations in response to speech: vocal imitation and developmental change. J. Acoust. Soc. Am. *100*, 2425–2438.

Landers, M., and Philip Zeigler, H. (2006). Development of rodent whisking: trigeminal input and central pattern generation. Somatosens. Mot. Res. *23*, 1–10.

Li, C.X., and Waters, R.S. (1991). Organization of the mouse motor cortex studied by retrograde tracing and intracortical microstimulation (ICMS) mapping. Can. J. Neurol. Sci. *18*, 28–38.

Matyas, F., Sreenivasan, V., Marbach, F., Wacongne, C., Barsy, B., Mateo, C., Aronoff, R., and Petersen, C.C. (2010). Motor control by sensory cortex. Science *330*, 1240–1243.

Mitchinson, B., Martin, C.J., Grant, R.A., and Prescott, T.J. (2007). Feedback control in active sensing: rat exploratory whisking is modulated by environmental contact. Proc. Biol. Sci. *274*, 1035–1041.

Mooney, R. (1992). Synaptic basis for developmental plasticity in a birdsong nucleus. J. Neurosci. *12*, 2464–2477.

Mooney, R., and Rao, M. (1994). Waiting periods versus early innervation: the development of axonal connections in the zebra finch song system. J. Neurosci. *14*, 6532–6543.

O'Connor, D.H., Clack, N.G., Huber, D., Komiyama, T., Myers, E.W., and Svoboda, K. (2010). Vibrissa-based object localization in head-fixed mice. J. Neurosci. *30*, 1947–1967.

Osakada, F., Mori, T., Cetin, A.H., Marshel, J.H., Virgen, B., and Callaway, E.M. (2011). New rabies virus variants for monitoring and manipulating activity and gene expression in defined neural circuits. Neuron *71*, 617–631.

Petreanu, L., Huber, D., Sobczyk, A., and Svoboda, K. (2007). Channelrhodopsin-2-assisted circuit mapping of long-range callosal projections. Nat. Neurosci. *10*, 663–668.

Petreanu, L., Mao, T., Sternson, S.M., and Svoboda, K. (2009). The subcellular organization of neocortical excitatory connections. Nature *457*, 1142–1145.

Sachdev, R.N., Berg, R.W., Champney, G., Kleinfeld, D., and Ebner, F.F. (2003). Unilateral vibrissa contact: changes in amplitude but not timing of rhythmic whisking. Somatosens. Mot. Res. *20*, 163–169.

Sellien, H., Eshenroder, D.S., and Ebner, F.F. (2005). Comparison of bilateral whisker movement in freely exploring and head-fixed adult rats. Somatosens. Mot. Res. *22*, 97–114.

Semba, K., and Egger, M.D. (1986). The facial "motor" nerve of the rat: control of vibrissal movement and examination of motor and sensory components. J. Comp. Neurol. *247*, 144–158.

Smith, J.C., Ellenberger, H.H., Ballanyi, K., Richter, D.W., and Feldman, J.L. (1991). Pre-Bötzinger complex: a brainstem region that may generate respiratory rhythm in mammals. Science *254*, 726–729.

Smith, J.C., Abdala, A.P., Rybak, I.A., and Paton, J.F. (2009). Structural and functional architecture of respiratory networks in the mammalian brainstem. Philos. Trans. R. Soc. Lond. B Biol. Sci. *364*, 2577–2587.

Stepien, A.E., Tripodi, M., and Arber, S. (2010). Monosynaptic rabies virus reveals premotor network organization and synaptic specificity of cholinergic partition cells. Neuron *68*, 456–472.

Tan, W., Janczewski, W.A., Yang, P., Shao, X.M., Callaway, E.M., and Feldman, J.L. (2008). Silencing preBötzinger complex somatostatin-expressing neurons induces persistent apnea in awake rat. Nat. Neurosci. *11*, 538–540.

Towal, R.B., and Hartmann, M.J. (2006). Right-left asymmetries in the whisking behavior of rats anticipate head movements. J. Neurosci. *26*, 8838–8846.

Ugolini, G. (1995). Specificity of rabies virus as a transneuronal tracer of motor networks: transfer from hypoglossal motoneurons to connected second-order and higher order central nervous system cell groups. J. Comp. Neurol. *356*, 457–480.

Wallace, P.S., and Whishaw, I.Q. (2003). Independent digit movements and precision grip patterns in 1-5-month-old human infants: hand-babbling, including vacuous then self-directed hand and digit movements, precedes targeted reaching. Neuropsychologia *41*, 1912–1918.

Welker, W.I. (1964). Analysis of sniffing of the albino rats. Behaviour *22*, 223–244.

Wickersham, I.R., Finke, S., Conzelmann, K.K., and Callaway, E.M. (2007a). Retrograde neuronal tracing with a deletion-mutant rabies virus. Nat. Methods *4*, 47–49.

Wickersham, I.R., Lyon, D.C., Barnard, R.J., Mori, T., Finke, S., Conzelmann, K.K., Young, J.A., and Callaway, E.M. (2007b). Monosynaptic restriction of transsynaptic tracing from single, genetically targeted neurons. Neuron *53*, 639–647.

Wineski, L.E. (1985). Facial morphology and vibrissal movement in the golden hamster. J. Morphol. *183*, 199–217.